Molecular Cell, Vol. 11, 91–102, January, 2003, Copyright ©2003 by Cell Press

Structural Basis of the Ribosomal Machinery for Peptide Bond Formation, Translocation, and Nascent Chain Progression

Anat Bashan,[1,5] Ilana Agmon,[1,5] Raz Zarivach,[1] Frank Schluenzen,[2] Joerg Harms,[2] Rita Berisio,[2,6] Heike Bartels,[2] Francois Franceschi,[3] Tamar Auerbach,[1,4] Harly A.S. Hansen,[2] Elizaveta Kossoy,[1] Maggie Kessler,[1] and Ada Yonath[1,2,*]

[1]Department of Structural Biology
Weizmann Institute
76100 Rehovot
Israel

[2]Max-Planck-Research Unit for Ribosomal Structure
Notkestrasse 85
22603 Hamburg
Germany

[3]Max-Planck-Institute for Molecular Genetics
Ihnestrasse 73

[4]FB Biologie, Chemie, Pharmazie
Frei University Berlin
Takustrasse 3
14195 Berlin
Germany

Summary

Crystal structures of tRNA mimics complexed with the large ribosomal subunit of *Deinococcus radiodurans* indicate that remote interactions determine the precise orientation of tRNA in the peptidyl-transferase center (PTC). The PTC tolerates various orientations of puromycin derivatives and its flexibility allows the conformational rearrangements required for peptide-bond formation. Sparsomycin binds to A2602 and alters the PTC conformation. H69, the intersubunit-bridge connecting the PTC and decoding site, may also participate in tRNA placement and translocation. A spiral rotation of the 3′ end of the A-site tRNA around a 2-fold axis of symmetry identified within the PTC suggests a unified ribosomal machinery for peptide-bond formation, A-to-P-site translocation, and entrance of nascent proteins into the exit tunnel. Similar 2-fold related regions, detected in all known structures of large ribosomal subunits, indicate the universality of this mechanism.

Introduction

Ribosomes are the macromolecular assemblies responsible for protein biosynthesis. These large riboprotein complexes are built of two unequal subunits (50S and 30S in prokaryotes) that associate upon the initiation of the protein biosynthesis process. Peptide-bond formation, the principal reaction of protein biosynthesis, was localized in the large subunit over three decades ago (Monro et al., 1968). Functional and protection studies indicated that peptidyl-transferase activity is associated predominantly with ribosomal RNA and that the peptidyl-transferase center (PTC) contains two highly conserved RNA features, called A and P loops, which accommodate the 3′ termini of A (aminoacyl) and P (peptidyl) tRNAs (Cundliffe, 1990; Moazed and Noller, 1991; Noller et al., 1992; Garrett and Rodriguez-Fonseca, 1995; Samaha et al., 1995). Crystal structures of complexes of *Thermus thermophilus* ribosomes (T70S) with tRNA (Yusupov et al., 2001) as well as of the large ribosomal subunits from the archaeon *Haloarcula marismortui* (H50S) and the mesophilic eubacterium *Deinococcus radiodurans* (D50S) with various substrate peptidyl-transferase analogs or inhibitors (Nissen et al., 2000; Schluenzen et al., 2001; Schmeing et al., 2002; Hansen et al., 2002) show that the PTC can be described as a pocket with a tunnel emerging from it. It is located at the bottom of a cavity containing all of the nucleotides known to bind the 3′-termini of the A- and the P-site tRNA molecules. Its front side is close to the subunit interface, and its rear wall spans from the A to the P site on the opposite side. The PTC pocket is vacant except for nucleotides A2602 (*E. coli* numbering system is used throughout the text) and U2585, which bulge into its center, leaving an arched void of a width sufficient to accommodate tRNA-3′ ends.

The PTC is highly conserved; nevertheless, variability in its structure was observed and it appears that PTC conformation may depend on several parameters, including the functional state of the ribosome. Nucleotides that show different orientations in the T70S-tRNAs complex and the liganded H50S include A2451, U2506, U2585, and A2602 (Yusupov et al., 2001); the latter was found to be disordered in unbound H50S (Nissen et al., 2000). Phylogenetic variations may also cause PTC diversity (Rodriguez-Fonseca et al., 2000). Varying PTC conformations were observed in *E. coli* ribosomes under different chemical conditions (e.g., Miskin et al., 1968; Bayfield et al., 2001), and crystallographic studies on complexes of H50S with puromycin derivatives showed that these short tRNA mimics are positioned in the PTC in conformations requiring rearrangements in order to participate in peptide-bond formation (Hansen et al., 2002).

In the course of peptide-bond formation, the A-site tRNA carrying the nascent chain passes into the P site and the deacylated P-site tRNA moves from the P site to the E (exit) site. This fundamental act in the elongation cycle, called translocation, may be performed by a straightforward translation (Rheinberger et al., 1981; Lill and Wintermeyer, 1987) or by incorporating intermediate hybrid states, in which the tRNA acceptor stem moves relative to the large subunit whereas the anticodon moves relative to the small one (Moazed and Noller, 1989; Noller et al., 2002). Regardless of the mechanism, translocation requires substantial motion of ribosomal features. Significant mobility, which may lead to disorder (Ban et al., 2000), was observed in features of the large subunit involved in ribosomal functions by cryo-EM

*Correspondence: ada.yonath@weizmann.ac.il
[5]These authors contributed equally to this work.
[6]Present address: Institute of Biostructures and Bioimages, CNR, 80138 Napoli, Italy.

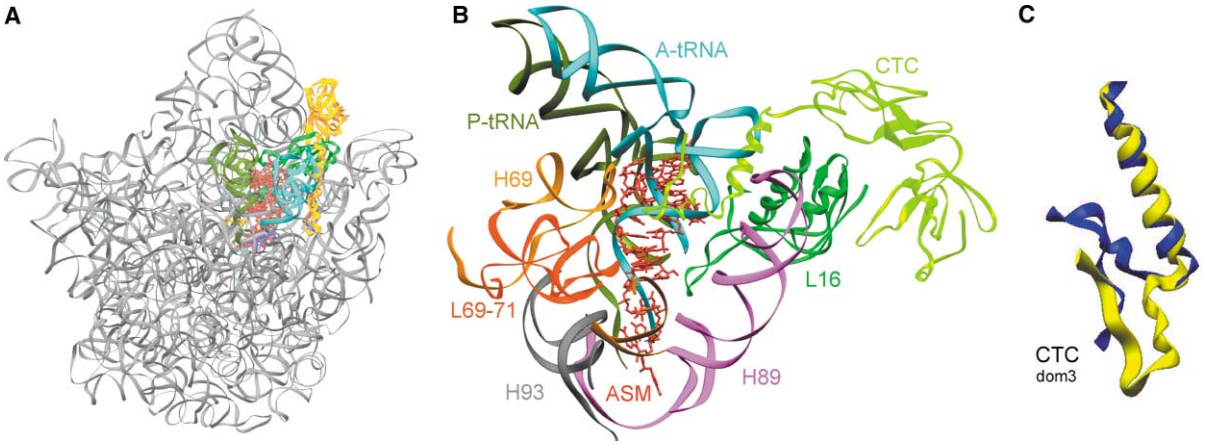

Figure 1. The PTC in the Large Ribosomal Subunit

(A) The location of the PTC within D50S (represented by its RNA backbone in gray). Shown are proteins L16 and CTC, ASM, ASM/SPAR, SPAR, and the docked A- and P-site tRNAs (color coded as in [B]).

(B) The PTC pocket, including ASM and of the docked A- and P-site tRNAs.

(C) The C-terminal domain of protein CTC (Harms et al., 2001) at its native (blue) and ASM bound (yellow) conformations.

(Frank and Agrawal, 2000), by comparing the crystal structures of the entire ribosome (Yusupov et al., 2001) with that of the unbound 50S subunit (Harms et al., 2001; Yonath, 2002).

Puromycin and sparsomycin are universal inhibitors of protein biosynthesis that exert their effects by interactions with the PTC. Puromycin resembles the 3′ terminus of aminoacyl-tRNA, but its aminoacyl residue is linked via an amide bridge rather than an ester bond. It played a central role in biochemical experiments aimed at understanding the mechanism of peptide-bond formation (e.g., Traut and Monro, 1964; Smith et al., 1965; Monro et al., 1968; Pestka, 1977; Vazquez, 1979; Gale et al., 1981; Bourd et al., 1983; Moazed and Noller, 1991; Noller et al., 1992; Porse and Garrett, 1995; Kirillov et al., 1997; Rodriguez-Fonseca et al., 1995, 2000). Puromycin binding in the presence of an active donor substrate can result in peptide-bond formation (Odom et al., 1990) uncoupled from movement of the A-site tRNA (Green et al., 1998). Since no further synthesis can take place, the peptidyl-puromycin falls off the ribosome.

Sparsomycin is a potent ribosome-targeted inhibitor that acts on all cell types, including Gram-positive bacteria and archae that are highly resistant to most antibiotics (Goldberg and Mitsugi, 1966; Vazquez, 1979; Cundliffe, 1981). In contrast to ribosome-targeted drugs, sparsomycin does not produce clear footprints on the 23S rRNA (Moazed and Noller, 1991). N-blocked aminoacyl-tRNAs appear to enhance its binding (Monro et al., 1969; Vazquez, 1979; Hornig et al., 1987; Lazaro et al., 1991; Moazed and Noller, 1991; Porse et al., 1999; Theocharis and Coutsogeorgopoulos, 1992). Although sparsomycin does not competitively inhibit A-site substrate binding, A-site antibiotics like chloramphenicol compete with it for binding to bacterial ribosomes. Mutants of A-site nucleotides increase the tolerance to sparsomycin (Lazaro et al., 1996; Tan et al., 1996), and crosslinks studies with sparsomycin derivatives were localized at A2602 (Porse et al., 1999).

Despite the wealth of biochemical information and the availability of crystal structures of ribosomal functional complexes, the molecular mechanism of peptidyltransferase activity is still not well understood. Biochemical and functional studies indicated that ribosomes facilitate peptidyl-transferase activity by providing the frame for accurate positioning of tRNA molecules (e.g., Cooperman, 1977; Nierhaus et al., 1980; Samaha et al., 1995; Pape et al., 1999; Polacek et al., 2001), and our previous results are consistent with this suggestion (Schluenzen et al., 2001; Harms et al., 2001; Yonath, 2002). In contrast, based on the crystal structure of complexes of H50S, it was proposed that ribosomes participate in the chemical catalysis of peptide-bond formation (Nissen et al., 2000). Doubts concerning this proposed mechanism arose from chemical and mutation experiments (Barta et al., 2001; Polacek et al., 2001; Thompson et al., 2001; Bayfield et al., 2001). These uncertainties were further substantiated by recent crystal structures of H50S complexes with additional substrate analogs (Hansen et al., 2002).

Here, we report the three-dimensional structures of complexes of D50S with substrate analogs mimicking the tRNA acceptor stem, the A-site tRNA CCA 3′ end, the antibiotic sparsomycin, and a combination of the tRNA acceptor-stem mimic and sparsomycin (ASM/SPAR). Analysis of these structures elucidated the binding modes of the substrate analogs and the inhibitors, illuminated dynamic elements in the PTC, indicated the presumed roles of B2a intersubunit bridge and base A2602, revealed a 2-fold axis in the PTC, and led us to suggest a ribosomal machinery for peptide-bond formation, translocation, and nascent protein progression.

Results and Discussion

Binding tRNA molecules to crystalline D50S led to a severe decrease in resolution. However, only a minor resolution change was observed in D50S crystals soaked in solutions containing tRNA acceptor stem mimics. The largest among these, ASM, is an RNA chain

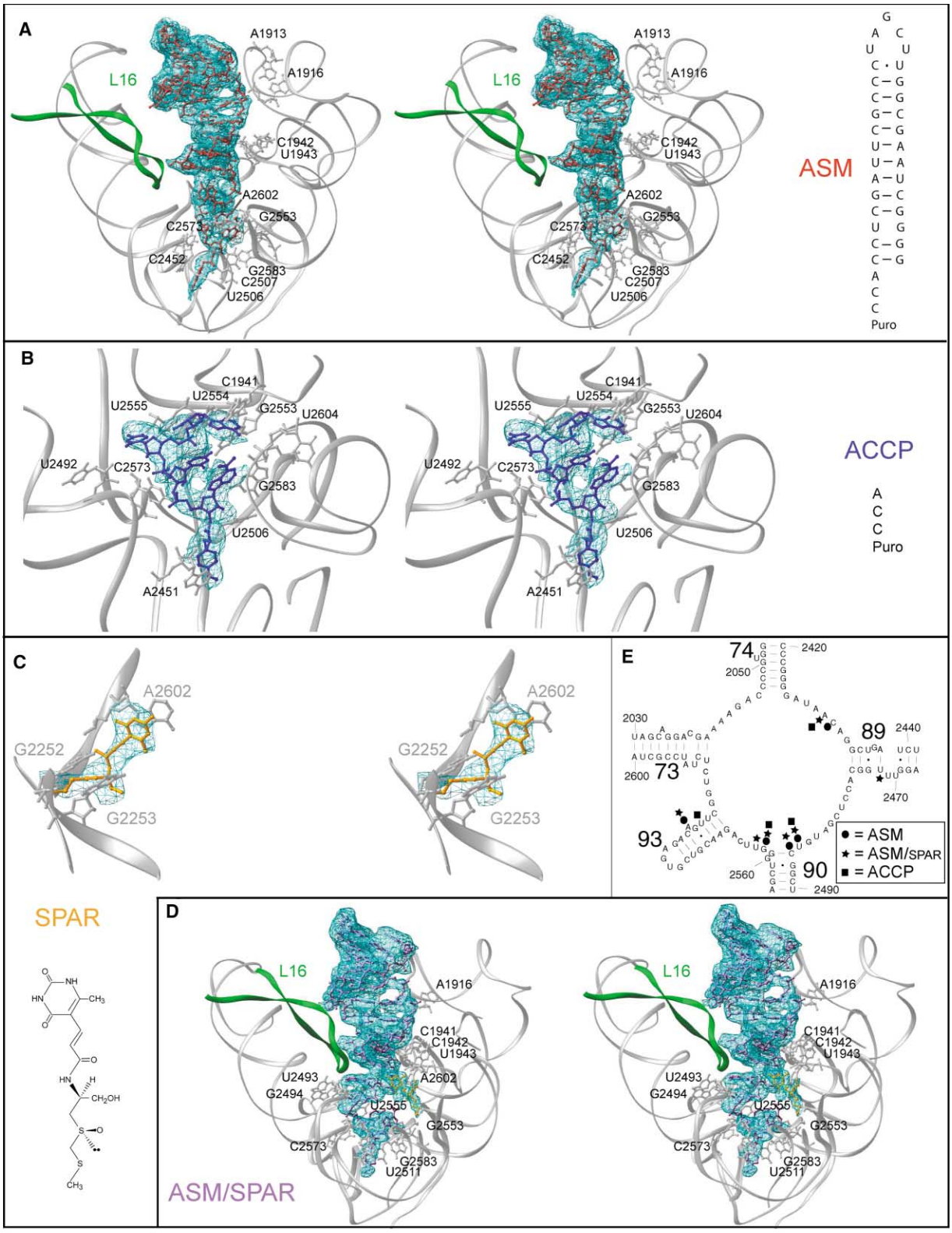

Figure 2. Substrate Analogs Bound to the PTC

(A–D) Stereo views showing the structures of ASM, ACCP, SPAR, and ASM/SPAR in their binding sites within D50S PTC, together with their electron density maps, contoured at 1.0σ. The sequences of ASM and ACCP and the chemical formula sparsomycin are inserted.

(E) Two-dimensional diagram of the 23S region of D50S PTC. The bases interacting with ASM, ACCP, and ASM/SPAR are marked.

Table 1. Crystallographic Statistics of Data Collection and Refinement

Crystal System	Resolution (Å)	Completeness (%)	I/Isig(I)	R_{sym} (%)	Number of Crystals	R Factor (%)	R_{free} (%)	Unit Cell (Å)
ASM	50.0-3.50	99.1	4.6	12.5	12	24.4	30.3	169.9
	3.63-3.50	96.8	2.1	38.4				409.9, 695.9
ACCP	50.0-3.70	97.8	7.9	15.6	4	28.3	30.5	169.9
	3.76-3.70	97.3	1.8	39.3				410.4, 697.1
SPAR	40.0-3.70	81.1	5.1	12.6	3	27.1	31.7	169.1
	3.76-3.70	80.0	1.7	37.0				409.9, 696.3
ASM/SPAR	50.0-3.60	95.2	5.8	16.9	7	28.4	32.6	169.6
	3.66-3.60	93.8	1.7	35.6				409.4, 695.1

Average standard deviations for bond lengths are 0.005 Å and bond angles 0.97°. Because of the high completeness, refinement was carried out using the data between 8 Å and the last shell. Numbers in the second row describe the highest resolution bin.

of 35 nucleotides, designed to represent the part of A-site tRNA that interacts with the large ribosomal subunit. Using the 3.0 Å structure of D50S (PDB entry 1NJW) as a starting model, the electron density maps of the ASM complex allowed us to define the D50S PTC pocket and to unambiguously localize 25 of the 35 nucleotides of ASM (Figures 1 and 2). Complexes of D50S with a short substrate analog, ACC-puromycin (called ACCP) and sparsomycin (called SPAR), and of cocrystals of D50S with sparsomycin soaked in solutions containing ASM (called ASM/SPAR), diffract to comparable resolution (Table 1) and led to interpretable electron density maps (Figure 2).

To allow correlation between the binding modes of tRNA (or its mimic) to unbound D50S and assembled 70S ribosome, the A- and the P-site tRNAs of the 5.5 Å structure of T70S complex (Yusupov et al., 2001) were docked onto D50S (Harms et al., 2001). The docking placed the A-site tRNA-3′ end in a location almost overlapping that of ASM 3′ end whereas the helical stem of ASM far end is somewhat displaced toward the P site (Figures 1B and 3A).

Remote Interactions of tRNA Are Key for Its Precise Positioning

Consistent with earlier findings (Eckerman and Symons, 1978; Vazquez, 1979; Hummel and Bock, 1987; Vester and Garrett, 1988; Mankin and Garrett, 1991), we found that the walls of the PT cavity are composed of RNA features. One of them is helix H69 that forms the B2a bridge (Yusupov et al., 2001; Harms et al., 2001). The features adjacent to H69 at the surface of the PTC cavity are helices H68, H70, H71, and H89. The bottom of the cavity consists of the backbone of nucleotides 2505–2506 and the bases of 2503–2504, 2451, and 2063. A2451 that, based on its location in H50S crystals, was implicated as a participant in peptide-bond formation catalytic mechanism (Nissen et al., 2000) does not interact with ASM in D50S, consistent with recent findings using other complexes of H50S (Hansen et al., 2002). Interestingly, protein CTC (Harms et al., 2001) that does not interact with ASM underwent substantial rearrangements (Figure 1) upon binding of the tRNA mimic, consistent with its presumed role in moderating A-site binding (Harms et al., 2001; Yonath, 2002).

The helical stem of ASM interacts with the extended loop of protein L16 and packs groove-to-backbone with H69 (Figure 3A). Hence H69 and L16 are likely to be the key factors influencing ASM stem positioning. Thus, tRNA mimics not held by remote interactions because they are too short (see below and in Schmeing et al., 2002, Hansen et al., 2002), or due to disorder in H69, as observed in H50S crystals (Ban et al., 2000, Nissen et al., 2000), bind to the PTC with orientations requiring conformational rearrangements for peptide-bond formation.

The B2a bridge interacts simultaneously with the small subunit decoding site and the PTC in the large one, thus connecting the two ribosomal active centers. In D50S, H69, the main feature of this bridge, is located at the intersubunit interface, and to create the intersubunit bridge it stretches toward the small subunit (Harms et al., 2001; Yonath, 2002). B2a's inherent flexibility and its proximity to both A and P sites suggest that it may also act as signal transmitter between the two active sites and participate in translocation as a carrier of the A-site tRNA acceptor stem (Figure 3C). Mapping of *E. coli*-modified nucleotides (Ofengand and Bakin, 1997) onto D50S structure showed clustering in the vicinity of the PTC and in the H69 stem loop, suggesting that they play a role in the bridging events.

Sparsomycin Triggers PTC Conformational Alterations

Like PTC antibiotics studied so far, namely chloramphenicol and clindamycin (Schluenzen et al., 2001), sparsomycin binds exclusively to 23S RNA. Stacking interactions between the sparsomycin-modified uracil ring and the highly conserved base A2602 that appear to be the sole contacts of sparsomycin (Figure 2C) are consistent with crosslinks produced by derivatized sparsomycin (Porse et al., 1999) and rationalize the difficulties of its localization in the ribosome (Monro et al., 1968; Vazquez, 1979; Lazaro et al., 1991; Moazed and Noller, 1991; Tan et al., 1996; Porse et al., 1999). SPAR binding mode to D50S is consistent with drug inactivation caused by derivatization of SPAR uracil ring and with the marginal loss of its inhibitory activity resulting by alteration of SPAR's second potentially reactive moiety, the sulfoxy group (Porse et al., 1999). It also explains why substitution of SPAR terminal methyl group did not decrease the yields of A2602 crosslinking (Lazaro et al., 1996; Porse et al., 1999). In its single binding site, sparsomycin is adjacent to two universally conserved guanosine residues, G2252 and G2253 (Gutell et al., 1993). Although its distances to these bases are too

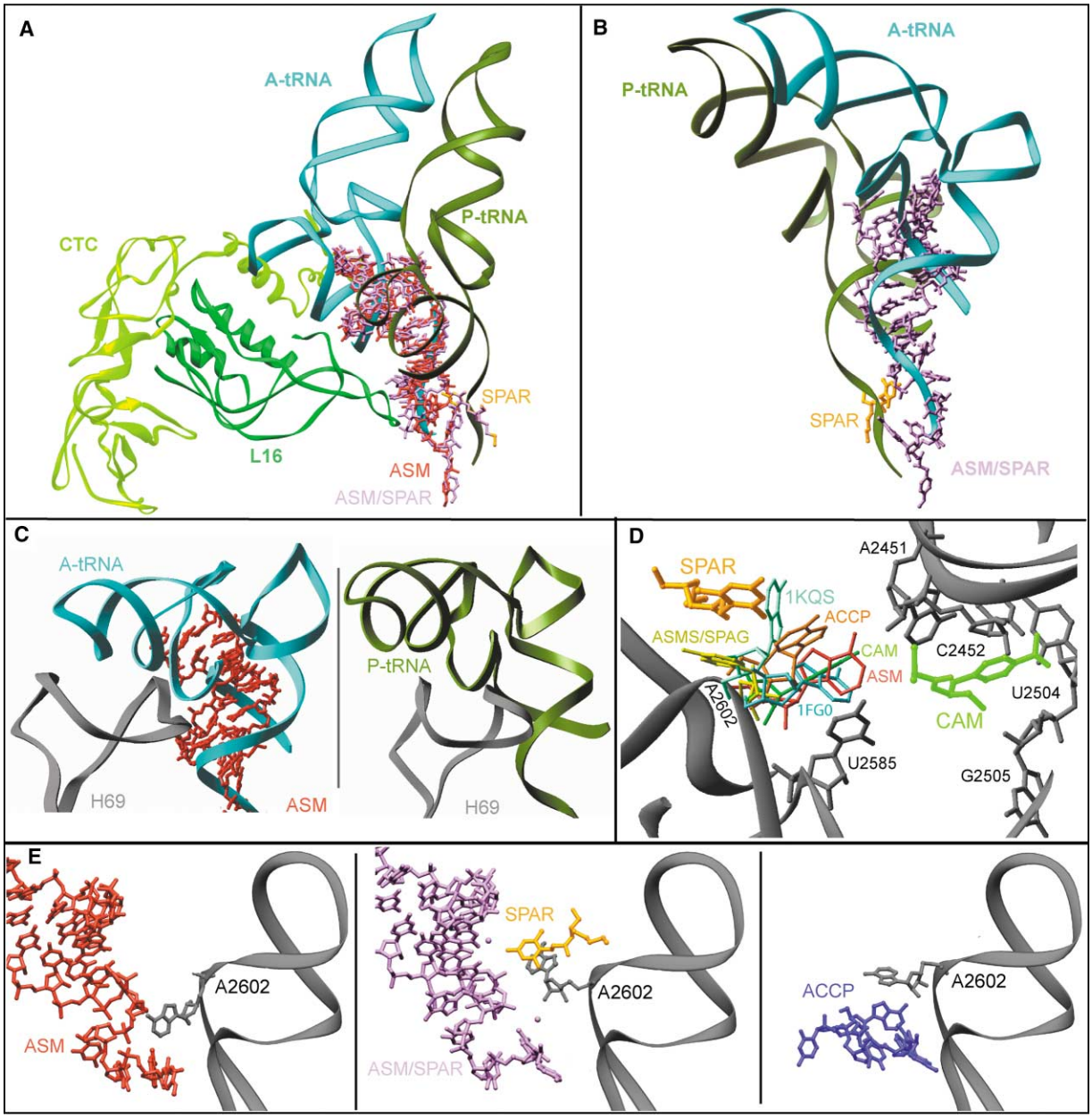

Figure 3. Flexibility within the PTC

(A and B) Side and front (compared to Figure 1A) views of the PTC. The view shown in (A) includes the docked A- and P-site tRNAs, ASM, ASM/SPAR, and SPAR. It highlights the contributions of protein L16 to the precise positioning of ASM and the proximity of protein CTC. The view in (B) shows SPAR and ASM/SPAR and their relative orientations compared to the docked A- and P-sites tRNA.

(C) H69 with ASM and the docked A-site tRNA in D50S (left) and together with P-site tRNA in T70S (right).

(D) The relative orientations of A2602 (A2581D) in different complexes of D50S (ASM, ASM/SPAR, ACCP) and H50S: PDB entry 1FGO (Nissen et al., 2000) and PDB entry 1KQS (Schmeing et al., 2002). The conformations of A2602 (A2581D) in D50S complexes with sparsomycin (SPAR) and chloramphenicol (CAM) were included to indicate the limits of A2602 flexibility.

(E) Three views, showing the backbone of H93 in the same orientation, together with ASM (left), SPAR (gold), and ASM/SPAR (middle) and ACCP (right). Hydrated Mg^{2+} ions are shown as pink dots.

long (~4.7 Å) for van der Waals contacts or for the formation of hydrogen bonds, the proximity of sparsomycin to these nucleotides may influence protein biosynthesis, as they were shown to be involved in peptide-bond formation (Moazed and Noller, 1989; Green et al., 1997).

Sparsomycin appears to significantly alter the conformation of both A and P sites, presumably via its contacts with A2602. This base undergoes the largest conformational rearrangements upon substrate and sparsomycin binding (Figure 3D), and since it is located in the center of the PTC and possesses unusual inherent flexibility, it seems to induce significant conformational rearrangements in the PTC. Among the nucleotides that

Table 2. Interactions of Substrate Analogs with the Ribosome

(A) tRNA Acceptor-Stem Mimic (ASM)

	ASM	(tRNA)	Helix/Loop	rRNA/Protein (*E. coli*)	Comments
1	G 01	(A05)		L16, aa79–81 (58–60)	Hydrophilic with protein loop. Missing in H50S
2	C 05 O2′	(A05)	H69	A 1899 O1P (A1916)	Missing in H50S
3	U 06 O2P	(U06)	H69	A 1896 N6 (A1913)	Missing in H50S
4	C 21 O2′	(C63)	H69	C 1892 O2′ (C1909)	Missing in H50S
5	U 29 O2′	(G71)	L69-71	U 1926 O2P (U1943)	Missing in H50S
6	U 29 O2	(G71)	L69-71	C 1925 O2′ (C1942)	Missing in H50S
7	C 30 O2′	(C72)	L69-71	C 1925 O4′ (C1942)	Missing in H50S
8	A 32 O2′	(A73)	H93	A 2581 N6 (A2602)	
9	C 33 N4	(C74)	H92	U 2534 O4 (U2555)	
10	C 34 N4	(C75)	H92	G 2532 O6 (G2553)	BP
11	C 34 N3	(C75)	H92	G 2532 N1 (G2553)	BP
12	C 34 O2	(C75)	H92	G 2532 N2 (G2553)	BP
13	C 34 O2	(C75)	H90	C 2486 O2′ (C2507)	
14	C 34 O3′	(C75)	H90	C 2552 N4 (C2573)	Missing in H50S[a]
15	PURO O2′	(A76)	L89-90	U 2485 O2′ (U2506)	
16	PURO O2′	(A76)	L89-90	U 2485 O2 (U2506)	
17	PURO O2′	(A76)	L90-93	G 2562 N2 (G2583)	
18	PURO N3′	(A76)	L89-90	U 2485 O2′ (U2506)	
19	PURO N3	(A76)	L90-93	G 2562 N2 (G2583)	
20	PURO N1	(A76)	L90-93	G 2562 O2′ (G2583)	
21	PURO–tyrosine ring	(A76)	L74-89	C 2431 (C2452)	Stacking

(B) ACC-Puromycin (ACCP)

	ACCP[b]	(tRNA)	Helix/Loop	rRNA/Protein (*E. coli*)	Comments
1	A 32 N7	(A73)	L69-71	C 1924 O2′ (C1941)	
2	A 32 N6	(A73)	H93	U 2583 O1P (U2604)	
3	A 32 O2′	(A73)	H92	U 2533 O4 (U2554)	
4	C 33 O1P	(C74)	H92	U 2533 N3 (U2554)	
5	C 33 N4	(C74)	H92	U 2534 O2′ (U2555)	
6	C 34 N4	(C75)	H92	G 2532 O6 (G2553)	BP
7	C 34 N3	(C75)	H92	G 2532 N1 (G2553)	BP
8	C 34 O2	(C75)	H92	G 2532 N2 (G2553)	BP
9	C 34 O2′	(C75)	H90	C 2552 N4 (C2573)	
10	PURO O2′	(A76)	L89-90	U 2485 O2 (U2506)	
11	PURO N3	(A76)	L90-93	G 2562 N2 (G2583)	
12	PURO N1	(A76)	L90-93	G 2562 O2′ (G2583)	
13	PURO N3′	(A76)	L89-90	U 2485 O2′ (U2506)	
14	PURO O	(A76)	L74-89	A 2430 O2′ (A2451)	

(C) tRNA Acceptor-Stem Mimic + Sparsomycin (ASM/SPAR)

	ASM/SPAR	(tRNA)	Helix/Loop	rRNA/Protein (*E. coli*)	Comments
1	G 01	(G01)		L16 aa79-81 (58-60)	
2	G 02 N3	(C02)		Mg 101	
3	C 05 O2′	(A05)	H69	A 1899 O1P (A1916)	
4	U 29 O2′	(G71)	L69-71	U 1926 O1P (U1943)	
5	C 30 O2′	(C72)	L69-71	C 1924 O2′ (C1941)	
6	C 31 O2′	(A73)	H93	A 2581 N3 (A2602)	
7	C 31 O2	(A73)		Mg 102	
8	C 33 O2′	(C74)	H89	U 2472 O3′ (U2493)	
9	C 33 N4	(C74)	H92	U 2534 O4 (U2555)	
10	C 34 N4	(C75)	H92	G 2532 O6 (G2553)	BP
11	C 34 N3	(C75)	H92	G 2532 N1 (G2553)	BP
12	C 34 O2	(C75)	H92	G 2532 N2 (G2553)	BP
13	C 34 O2	(C75)	H90	C 2486 O2′ (C2507)	
14	C 34 O2′	(C75)	H90	C 2486 O2′ (C2507)	
15	C 34 O3′	(C75)	H90	C 2552 N4 (C2573)	
16	PURO O2′	(A76)	L90-93	U 2485 O2 (U2508)	
17	PURO O2′	(A76)	L90-93	U 2563 O2′ (U2582)	
18	PURO N3	(A76)	L90-93	G 2562 N2 (G2583)	
19	PURO O5′	(A76)	H90	C 2552 N4 (C2573)	
20	PURO O	(A76)	L74-89	A 2430 O2′ (A2451)	
21	PURO N	(A76)	L74-89	A 2430 O2′ (A2451)	
22	PURO N	(A76)	L74-89	A 2430 N3 (A2451)	

Contacts missing in H50S due to the disorder of the tRNA mini-helix are noted.

[a] Contacts missing in H50S, although this part is seen in the map.

[b] The numbering of the ACCP bases is according to the numbering of the ASM mimic.

alter their conformations upon sparsomycin binding, some are distant from SPAR but may interact with A2602 in its various conformations. These include A2438, C2452, C2499, U2500, and U2584 that were implicated in A-site binding, and their single-site mutations show enhancement of sparsomycin resistance (Tan et al., 1996). The SPAR-induced conformational rearrangements within the A site explain its competition with chloramphenicol although they do not share overlapping positions (Lazaro et al., 1991; Tan et al., 1996), and we conclude that sparsomycin inhibits protein biosynthesis by introducing substantial alterations of the conformation of the PTC.

SPAR stacking interactions with A2602 seem to be sufficient for its firm attachment as long as the large subunit is not involved in protein biosynthesis or in other functional tasks requiring the participation of A2602. Destabilization of SPAR binding during protein biosynthesis may be correlated to orientation alterations of its counterpart, A2602, that was implicated to play an active role in protein biosynthesis. Consistent with SPAR location in D50S is its tighter binding in the presence of N-blocked aminoacyl-tRNAs at the P site (Porse et al., 1999). The binding enhancement of SPAR by N-blocked aminoacyl-tRNA may indicate that SPAR inhibits protein biosynthesis not only by altering the PTC conformation but also by trapping nonproductive intermediate-state compounds.

The binding fashion of ASM/SPAR is shown in Figure 3B. Although ASM in the ASM/SPAR complex is placed closer to the P site than ASM alone, in both complexes ASM makes a comparable number of contacts with 23S RNA. However, ASM/SPAR maintains only 11 out of the 21 ASM interactions (Table 2). Two additional contacts of ASM/SPAR involve bases that interact with ASM, but in a different fashion. Among the contacts common to ASM and ASM/SPAR is the base pair C34 (tRNA C75) with G2553. Interactions unique to ASM/SPAR are with H89 and the PTC region between H74 and H89. Since the ASM/SPAR structure was determined using crystals obtained by soaking D50S/SPAR crystals in solutions containing ASM, it appears that the difference between ASM and ASM/SPAR binding modes results from PTC alterations triggered by SPAR binding, presumably via its contacts with A2602. In the complex of H50S with SPAR and a P-site substrate analog (Hansen et al., 2002), A2602 is placed somewhat differently than in D50S, and whereas in H50S SPAR faces the A site, in D50S complexes with SPAR or ASM/SPAR it points toward the P site. Differences in sparsomycin binding in different kingdoms were reported previously (Lazaro et al., 1991) and may be the reason for these findings. Alternatively, the differences in SPAR binding in the two crystal systems may reflect the experimental procedures, since in the D50S case ASM was added to the starting crystals that contained pre-formed complexes of D50S/SPAR, whereas the H50S complex was obtained by soaking H50S crystals in solutions containing both SPAR and the P-site complex (Hansen et al., 2002).

The PTC Tolerates Various Binding Modes

The orientations of ASM, ACCP, and ASM/SPAR within the PTC are similar but show notable variations. None of their orientations is identical to any of the orientations observed for the H50S analogs. Table 2 and Figure 2B show the ACCP interactions with D50S, most of which are consistent with crosslinking results (Hall et al., 1988; Kirillov et al., 1999). However, the ASM 3′ end shares only 6 of the 14 ACCP interactions, including the base pair between G2553 and C34 (tRNA C75), the contacts between C33 (tRNA C74) and U2555, and the contacts of the puromycin end with G2583 and U2506. For the latter, the chemical nature of the interactions is different. G2583 shows the largest variability. It lies almost perpendicular to ASM but packs side-to-side with ACCP. Nucleotide C2573 interacts with both compounds, but in a slightly different fashion. Three nucleotides, C2507, G2452, and A2602, interact only with ASM, and four nucleotides, C1941, A2451, U2554, and U2604, make contacts with ACCP but not with the 3′ end of ASM.

The Watson-Crick base pair between ASM or ACCP C34 (tRNA C75) and G2553 (Kim and Green, 1999) appears to be a common feature in all D50S complexes, in the T70S/tRNA complex (Yusupov et al., 2001), and in the liganded H50S (Nissen et al., 2000; Schmeing et al., 2002; Hansen et al., 2002). In contrast, the contacts made by C33 (tRNA C74) of ASM and ACCP with U2555 of D50S are not seen in H50S crystal structures, where this base is stacked with U2554. Furthermore, in H50S, A76 of the ligand induces shifts in three bases, U2585, U2584, and G2583, whereas the equivalent base in both ASM and ACCP does not induce rearrangements in D50S and makes different contacts with it (Table 2).

A2602 is the PTC nucleotide that undergoes the largest conformational changes upon binding of substrates or inhibitors. As a consequence, it has a different orientation in each of the complexes studied by us or by others (Figure 3D). In the complex of ASM with D50S, A2602 has similar conformations to that of the D50S native structure. In both, it is located in the middle of the PTC, within contact distance with ASM and the docked tRNAs. In the ACCP/D50S complex, it also points into the PTC center but has a slightly different orientation. In both SPAR and ASM/SPAR structures, A2602 points toward the P site and acquires a distinctly different orientation. Combining the structures reported here and in Nissen et al. (2000), Schluenzen et al. (2001), and Schmeing et al. (2002), we demonstrate that A2602 can undergo a flip of $\sim$180° (Figure 3D). In all these complexes, A2602 is located within the space between its locations in D50S/SPAR and D50S/chloramphenicol (Schluenzen et al., 2001). A2602 is the only nucleotide in the PTC that possesses such striking diversity. This great variability suggests that A2602 takes part in the A- to P-site passage and plays a dynamic role in translocation, likely to be in concert with H69. While the latter assists the translocation near the subunit interface, the A2602 serves as a conformational switch within the PTC.

Two-Fold Rotation Axis in the PTC

Analysis of D50S PTC revealed an approximate 2-fold symmetry (Figure 4), consistent with the observation that the 3′ termini of tRNA and puromycin derivatives are related by rotation (Nissen et al., 2000, Yusupov et al., 2001, Schmeing et al., 2002, Hansen et al., 2002), although the tRNA helical features are related by transla-

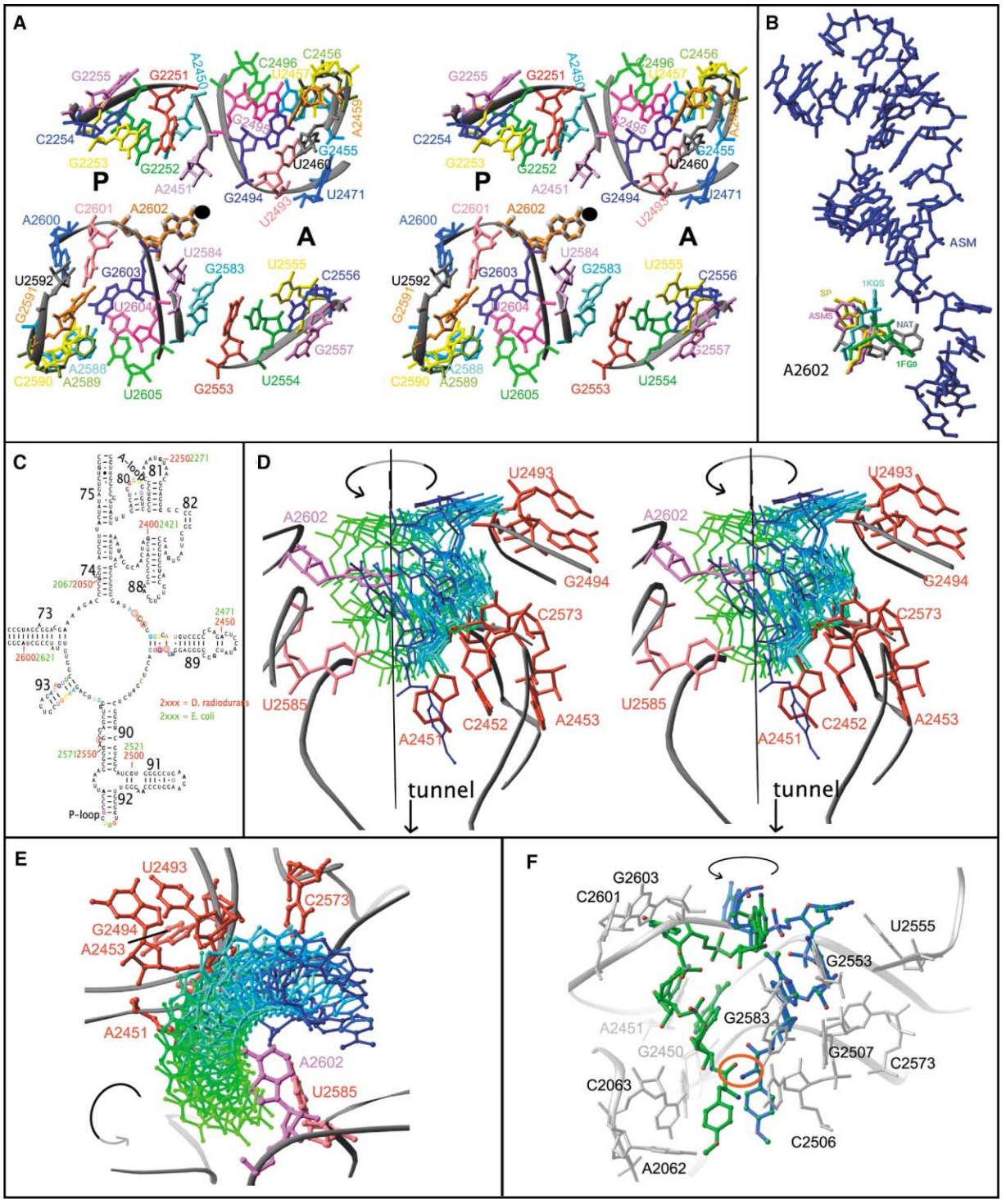

Figure 4. Two-Fold Rotation and Peptide Bond Formation

(A) A projection down the 2-fold axis of the 2-fold symmetry-related region in D50S PTC. The 2-fold axis is marked by a black circle. Symmetry-related nucleotides are colored identically. Key for conversion to *E. coli* system is given in (C).

(B) Selected positions of A2602 in relation to the tRNA acceptor stem mimic. 1FG0 and 1KQS are the PDB entries of H50S complexes with substrate analogs, docked onto D50S structure.

(C) The 2D diagram of D50S nucleotides involved in the proposed mechanism. Related nucleotides are colored as in (A). Rear-wall nucleotides are circled in red.

(D and E) Snapshots of the spiral motion, obtained by successive rotations of 15° each around the 2-fold axis, coupled with the appropriate fraction of the total translation. Shown are orthogonal views of tRNA-3′ end passage from A to P site, represented by the transition from blue (A-site aminoacylated tRNA) to green (P-site leaving group). The PTC backbone is shown in gray. The rear-wall nucleotides are shown in red and the anchors in magenta and pink. The black line represents the 2-fold rotation axis; an arrow shows the rotation direction. (D) A stereo view perpendicular to the 2-fold axis. (E) A projection from the PTC upper end (in relation to Figure 1B) down the 2-fold axis. A73 was removed because of its proximity to the rotation axis.

(F) The relative positions of the A-site (blue) primary amino and P-site (green) carboxyl groups that should participate in peptide-bond formation (encircled in red).

tion (Stark et al., 1997; Yusupov et al., 2001). The detection of 2-fold symmetry in all known structures of ribosomal large subunits verified its universality and prompted the identification of a 2-fold rotation axis within the PTC. The presumed functional relevance of inherent 2-fold symmetry within the active site of the ribosome, a particle that appears to lack any other internal symmetry, and the high sequence conservation of the PTC rear-wall nucleotides (defined in Figure 4C), led us to suggest a simple machinery for peptide-bond formation, translocation, and the entrance of nascent proteins into the exit tunnel. According to this mechanism, the tRNA A- to P-site passage involves two independent motions: a spiral rotation of ~180° of the A-site tRNA-3′ end, performed in conjunction with peptide-bond formation, and A- to P-site translation of the tRNA acceptor stem. In support of sovereign motions of tRNA structural features is the suggested hybrid-state translocation mechanism (Moazed and Noller, 1989; Noller et al., 2002).

The approximate 2-fold axis is located at the PTC center. It relates backbone fold and nucleotide conformation of two groups of at least seventeen nucleotides each (Figure 4A), the majority of which are located in the PTC upper rims. These nucleotides form two belts, each held at one end by a double helix (H89 and H93). One group includes five A-loop nucleotides, most of helix H93, and two nucleotides from domain V central loop. The second group contains the equivalent P loop nucleotides, part of helix H89, and two nucleotides on the opposite side of domain V central loop. We defined the core of the symmetry-related region as the space located within 14 Å from the 2-fold axis and found that most of the nucleotides within this core are highly conserved.

The P-O3′ bond between the single-strand 3′ end and the helical acceptor stem (tRNA 72–73) of the docked A-site tRNA and of ASM nearly overlaps the 2-fold axis. We therefore defined the rotating moiety (RM) as the entire single-strand 3′ end, namely tRNA bases 73–76. We found that the PTC 2-fold related environments allow similar, albeit not identical, interactions with the 3′ ends of the A- and the P-site tRNAs. We observed that the A-site base pair shared by all known structures, A-tRNA-C75 to G2553, can be formed in the symmetry-related region, with G2251, and the derived P-site tRNA can interact with the PTC in a manner consistent with most of the available biochemical data (Green et al., 1997). The rms deviations within couples of symmetrical nucleotides range between 0.1–1.4 Å. The nucleotides located at the edges of the A and P loops, 2556-7 and 2254-5, respectively, can be well superimposed on each other, whereas noticeable differences are found between 2554-5 and 2252-3. The former contact C74 of the docked tRNAs and ASM in D50S, as well as their mates in H50S, although these two PTC structures differ (Harms et al., 2001, Schluenzen et al., 2001) and although in H50S these nucleotides undergo conformational changes upon analogs binding (Nissen et al., 2000).

The 2-fold symmetry has a spiral nature, resulting from slightly deeper locations of several P-site nucleotides compared to their A-site mates. To examine the spiral path, we monitored the entire motion of RM (Figures 4D and 4E) and found no clashes throughout the rotation and no conformational adjustments were required (I.A., A.B., R.Z., and A.Y, unpublished data). The motion starts with A-site tRNA forming a base pair with G2553 and interacting with U2506, C2507, U2555, C2573, and G2583 (Table 1). While rotating, RM interacts with the bases of nucleotides C2573, A2451, C2452, and C2493 and slide along G2494 phosphate, the position of which is stabilized by the adjacent A-minor motif with H39 and a noncanonical base pair with U2457. At the P site, the RM is positioned so that its C74 interacts with 2601-3, C75 is base paired with G2251, and A76 interacts with G2063, A2450, and U2585. Although initially we treated the RM as a rigid body, in subsequent examinations we allowed deviations from rigidity, consistent with the known flexibility of tRNA-3′ ends. We found that the guidance of the rear-wall nucleotides together with the front anchoring restrict the possible motions of the RM nucleotides and limit their flexibility.

Two nucleotides interact with RM near the small subunit interface: A2602, whose N1 atom sits on the 2-fold axis and is within contact distances to tRNA-A73 throughout the rotation, and U2585, located below A2602, with its O4 close to the 2-fold axis and its base interacting with the rotated A76. We found that the space available for A2602 throughout the motion can accommodate its various conformations (Figures 3D and 4B), and it is conceivable that A2602 conformational changes are synchronized with the RM rotation. The T70S crystal structure (Yusupov et al., 2001) hints that tRNA-A73 is translated from A to P site together with tRNA acceptor stem, implying that the rotated moiety is C74-A76 rather than A73-A76. Our suggested motion holds for this case, but this rotating moiety will not be anchored to A2602, and the rotation will be simultaneous with the acceptor stem translation.

A Unified Ribosomal Machinery

Besides facilitating translocation, an additional biological implication of the suggested motion is a mild push of the nascent chain into the exit tunnel, likely to assist its progression. Thus, the P-site nucleotides G2251 and A2450 that interact with the P-site tRNAs C75 and A76, respectively, are located at the bottom of the PTC in a configuration ensuring that the translocation motion into the P site will deliver the peptidyl to the tunnel entrance.

The most significant biological implication of the 2-fold rotation is the favorable geometry between the moieties participating in peptide-bond formation (Figure 4F). Thus, the guidance of the A-site motion by the PTC nucleotides leads to orientation and distance suitable for a nucleophilic attack of the A-site primary amine on the P-site tRNA carbonyl-carbon. Such an attack should readily occur at the optimal pH for protein biosynthesis by most ribosomes (pH = 7.2–7.8), including *D. radiodurans* (Miskin et al., 1968; Shevack et al., 1985; Moazed and Noller, 1989, 1991; Noller et al., 1992; Rodriguez-Fonseca et al., 2000; Bayfield et al., 2001, Harms et al., 2001). We propose that the A- to P-site rotation is synchronized with peptide-bond formation, or triggered by it. The rotated A-site tRNA-3′ end replaces the P-site tRNA-3′ end, thus assisting the release of the P-site leaving group, and the translocation of the acceptor stems of both tRNAs should free space for binding the

next aminoacyl tRNA. The sole geometrical requirement for our proposed machinery is that the P-site tRNA in the initiation complex has its 3′ end in a conformation related to that of incoming A site by an approximate 2-fold rotation.

The existence of symmetry-related regions in all known PTC structures, the provision for ensured mild push of nascent proteins into the tunnel; the resulting mutual orientation of A- and P-site tRNAs suitable for peptide-bond formation, are consistent with the universality of our proposed machinery. This tentative machinery suggests a spontaneous peptide bond formation, consistent with results of previous biochemical experiments (Cooperman, 1977; Nierhaus et al., 1980; Moazed and Noller, 1989, Wilson and Noller, 1998) and requires precise positioning of tRNA in the PTC. Less optimal binding geometry of tRNA mimics may lead to the formation of a single peptide bond, which is not accompanied by A- to P-site passage; hence no further protein biosynthesis can take place. An example is the fragment assay performed within H50S crystals that led to an A-site bound product that was not passed to the P site (Schmeing et al., 2002), presumably because its geometry was not suitable for the spiral motion. Similarly, application of this motion to ASM/SPAR led to a P site placement requiring a significant conformational rearrangement in order to reach an orientation suitable for peptide bond formation, and we suggest that this reflects the inhibitory mechanism of sparsomycin.

Conclusions

We showed that precise positioning of tRNA within the PTC, which seems to be crucial for protein biosynthesis, is determined by the positioning of the tRNA helical stem, rather than by its 3′ end. Remote interactions with 23S RNA and protein L16 are the main contributors to the tRNA positioning. In the absence of these interactions, conformational rearrangements of the substrate are required to adopt an orientation that is suitable for peptide bond formation, and the inherent flexibility of the PTC may assist these rearrangements. H69, the intersubunit bridge connecting the PTC with the decoding center, is part of the PTC walls and may be involved in tRNA placement and translocation. Sparsomycin binds to an extremely flexible nucleotide located at the PTC center and inhibits protein biosynthesis by altering the PTC conformation. Segments of the PTC form a scaffold that guide the motion from A to P site, presumably by rotating around an internal 2-fold axis of symmetry observed within the PTC of all known structures.

Experimental Procedures

Numbering

Throughout the text, the nucleotides are numbered as in *E. coli*. Key for transformation to *E. coli* system is given in Figure 4C.

Crystals

D50S crystals of space-group I222 were grown from the large ribosomal subunits from *Deinococcus radiodurans* as described (Harms et al., 2001). SPAR crystals were obtained by cocrystallization of D50S in the presence of 10-fold excess of sparsomycin. ASM crystals were obtained by soaking D50S crystals in solution containing 0.025 mM of the tRNA acceptor stem mimic, an RNA chain of 35 nucleotides, with the sequence: 5′GGGGCUAAGCGGUUCGAUCC CGCUUAGCUCCACCPuro. The terminal C of ASM was coupled via a phosphodiester bond to the 5′ OH of the N6-dimethyl moiety of puromycin. ACCP crystals were obtained by soaking D50S crystals in solutions containing 0.0125 mM ACCP, which is a RNA chain of the sequence ACC. The terminal C was coupled via a phosphodiester bond to the 5′ OH of the N6-dimethyl moiety of puromycin. ASM/SPAR crystals were obtained by soaking SPAR crystals in solutions containing 0.025 mM ASM.

X-Ray Diffraction

Data were collected at 85 K from shock-frozen crystals with a bright SR beam at ID19 at APS/SBC/ANL and ID14/ESRF. Data were recorded on Quantum 4 or on the APS-CCD detectors and processed with HKL2000 (Otwinowski and Minor, 1997).

Placements and Refinement

The 3.0 Å structure of D50S was refined against the structure factor amplitudes of each of the complexes, using rigid body refinement as implemented in CNS (Brunger et al., 1998). SigmaA weighted difference maps were used for the initial manual placement of the substrate analogs or the sparsomycin. The coordinates of sparsomycin were obtained by energy minimization using the Discover module of INSIGHTII (Accelrys Inc., San Diego, CA). Each of the D50S-ligand models was further refined in CNS. For the calculation of free R factors (as reported in Table 1), a subset of reflections (5% of the data) was omitted from the refinement.

Definition of the 2-Fold Axis

Initially, the 2-fold axis was detected visually. For its quantitative definition, a transformation matrix was calculated, using LSQKAB (Bailey, 1994), first for the couple G2553/2251, and then verified by re-calculating it for each of the symmetry-related nucleotide-couples of D50S. The spiral rotation was found to be composed of 176–180° rotation and ~2.5 Å translation toward the tunnel. The direction-cosines of the 2-fold rotation axis are 0.98, −0.02, and −0.19 in D50S coordinate system, and most of the rotation axes of the 17 nucleotide-couples lie within a 12° cone. Rotation axes computed for all of the structures determined by us showed negligible accumulated variability.

Acknowledgments

We thank J.M. Lehn, M. Lahav, P. Fucini, A. Mankin, and W. Traub for critical discussions; R. Albrecht, D. Baram, W.S. Bennett, E. Ben-Zeev, H. Burmeister, R. Chen, C. Glotz, M. Laschever, C. Liebe, M. Peretz, C. Stamer, and A. Wolff for contributing to these studies; and the staff of ID19/SBC7APS/ANL and ID14-2 and ID14-4/ESRF/EMBL for their cooperation and assistance. The Max-Planck Society, the US National Institutes of Health (GM34360), the German Ministry for Science and Technology (BMBF Grant 05-641EA), and the Kimmelman Center for Macromolecular Assembly at the Weizmann Institute provided support. A.Y. holds the Helen and Martin Kimmel Professorial Chair.

Received: July 16, 2002
Revised: November 1, 2002

References

Bailey, S. (1994). The CCP4 suite: programs for protein crystallography. Acta Crystallogr. D *50*, 760–763.

Ban, N., Nissen, P., Hansen, J., Moore, P.B., and Steitz, T.A. (2000). The complete atomic structure of the large ribosomal subunit at 2.4 Å resolution. Science *289*, 905–920.

Barta, A., Dorner, S., and Polacek, N. (2001). Mechanism of ribosomal peptide bond formation. Science *291*, 203.

Bayfield, M.A., Dahlberg, A.E., Schulmeister, U., Dorner, S., and Barta, A. (2001). A conformational change in the ribosomal peptidyltransferase center upon active/inactive transition. Proc. Natl. Acad. Sci. USA *98*, 10096–10101.

Bourd, S.B., Kukhanova, M.K., Gottikh, B.P., and Krayevsky, A.A.

(1983). Cooperative effects in the peptidyltransferase center of *Escherichia coli* ribosomes. Eur. J. Biochem. *135*, 465–470.

Brunger, A.T., Adams, P.D., Clore, G.M., DeLano, W.L., Gros, P., Grosse-Kunstleve, R.W., Jiang, J.S., Kuszewski, J., Nilges, M., Pannu, N.S., et al. (1998). Crystallography & NMR system: a new software suite for macromolecular structure determination. Acta Crystallogr. D Biol. Crystrallogr. *54*, 905–921.

Cooperman, B.S. (1977). Identification of binding sites on the *E. coli* ribosome by affinity labeling, Adv. Exp. Med. Biol. *86A*, 595–609.

Cundliffe, E. (1981). Antibiotic inhibitors of ribosome function, E.F. Gale, E. Cundliffe, P.E. Reynolds, M.H. Richmond, and M. H. Waring, eds. (London, NY, Sydney, Toronto: Wiley).

Cundliffe, E. (1990). Recognition sites for antibiotics within rRNA. In The Ribosome: Structure, Function and Evolution, W.E. Hill, A.E. Dahlberg, R.A. Garrett, P.B. Moore, D. Schlessinger, and J.R. Warner, eds. (Washington, DC: ASM), pp. 479–90.

Eckerman, D.J., and Symons, R.H. (1978). Sequence at the site of attachment of an affinity-label derivative of puromycin on 23S ribosomal RNA of *E. coli* ribosomes. Eur. J. Biochem. *82*, 225–234.

Frank, J., and Agrawal, R.K. (2000). A ratchet-like inter-subunit reorganization of the ribosome during translocation. Nature *406*, 318–322.

Gale, E.F., Cundliffe, E., Reynolds, P.E., Richmond, M.H., and Waring, M.J. (1981). The Molecular Basis of Antibiotic Action (London: Wiley).

Garrett, R.A., and Rodriguez-Fonseca, C. (1995). The peptidyltransferase center. In Ribosomal RNA: Structure, Evolution, Processing and Function. R.A. Zimmermann and A.E. Dahlberg, eds. (Boca Raton: CRC Press), pp. 327–355.

Goldberg, I.H., and Mitsugi, K. (1966). Sparsomycin, an inhibitor of aminoacyl transfer to polypeptide. Biochem. Biophys. Res. Commun. *23*, 453–459.

Green, R., Samaha, R.R., and Noller, H.F. (1997). Mutations at nucleotides G2251 and U2585 of 23S rRNA perturb the peptidyltransferase center of the ribosome. J. Mol. Biol. *266*, 40–50.

Green, R., Switzer, C., and Noller, H.F. (1998). Ribosome-catalyzed peptide-bond formation with an A-site substrate covalently linked to 23S ribosomal RNA. Science *280*, 286–289.

Gutell, R.R., Gray, M.W., and Schnare, M.N. (1993). A compilation of large subunit (23S and 23S-like) ribosomal RNA structures: 1993. Nucleic Acids Res. *21*, 3055–3074.

Hall, C.C., Johnson, D., and Cooperman, B.S. (1988). [3H]-p-azidopuromycin photoaffinity labeling of *E. coli* ribosomes: evidence for site-specific interaction at U-2504 and G-2502 in domain V of 23S ribosomal RNA. Biochemistry *27*, 3983–3990.

Hansen, J.L., Schmeing T.M., Moore, P.B., and Steitz, T.A. (2002). Structural insights into peptide bond formation. Proc. Natl. Acad. Sci. USA *99*, 1670–1675.

Harms, J., Schluenzen, F., Zarivach, R., Bashan, A., Gat, S., Agmon, I., Bartels, H., Franceschi, F., and Yonath, A. (2001). High-resolution structure of the large ribosomal subunit from a mesophilic eubacterium. Cell *107*, 679–688.

Hornig, H., Woolley, P., and Luhrmann, R. (1987). Decoding at the ribosomal A site: antibiotics, misreading and energy of aminoacyl-tRNA binding. Biochimie *69*, 803–813.

Hummel, H., and Bock, A. (1987). 23S ribosomal RNA mutations in halobacteria conferring resistance to the anti-80S ribosome targeted antibiotic anisomycin. Nucleic Acids Res. *15*, 2431–2443.

Kim, D.F., and Green, R. (1999). Base-pairing between 23S rRNA and tRNA in the ribosomal A site. Mol. Cell *4*, 859–864.

Kirillov, S., Porse, B.T., Vester, B., Woolley, P., and Garrett, R.A. (1997). Movement of the 3′-end of tRNA through the peptidyl transferase centre and its inhibition by antibiotics. FEBS Lett. *406*, 223–233.

Kirillov, S.V., Porse, B.T., and Garrett, R.A. (1999). Peptidyltransferase antibiotics perturb the relative positioning of the 3′-terminal adenosine of P/P'-site-bound tRNA and 23S rRNA in the ribosome. RNA *5*, 1003–1013.

Lazaro, E., van den Broek, L.A., San Felix, A., Ottenheijm, H.C., and Ballesta, J.P. (1991). Biochemical and kinetic characteristics of the interaction of the antitumor antibiotic sparsomycin with prokaryotic and eukaryotic ribosomes. Biochemistry *30*, 9642–9648.

Lazaro, E., Rodriguez-Fonseca, C., Porse, B., Urena, D., Garrett, R.A., and Ballesta, J.P. (1996). A sparsomycin-resistant mutant of *Halobacterium salinarium* lacks a modification at nucleotide U2603 in the peptidyl transferase centre of 23S RNA. J. Mol. Biol. *261*, 231–238.

Lill, R., and Wintermeyer, W. (1987). Destabilization of codon-anticodon interaction in the ribosomal exit site. J. Mol. Biol. *196*, 137–148.

Mankin, A.S., and Garrett, R.A. (1991). Chloramphenicol resistance mutations in the single 23S rRNA gene of the archaeon *H. halobium*. J. Bacteriol. *173*, 3559–3563.

Miskin, R., Zamir, A., and Elson, D. (1968). The inactivation and reactivation of ribosomal-peptidyltransferase of *E. coli*. Biochem. Biophys. Res. Commun. *33*, 551–557.

Moazed, D., and Noller, H.F. (1989). Intermediate states in the movement of transfer RNA in the ribosome. Nature *342*, 142–148.

Moazed, D., and Noller, H.F. (1991). Sites of interaction of the CCAa end of peptidyl-transfer RNA with 23S ribosomal-RNA. Proc. Natl. Acad. Sci. USA *88*, 3725–3728.

Monro, R.E., Cerna, J., and Marcker, K.A. (1968). Ribosome-catalyzed peptidyl transfer: substrate specificity at the P-site. Proc. Natl. Acad. Sci. USA *61*, 1042–1049.

Monro, R.E., Celma, M.L., and Vazquez, D. (1969). Action of sparsomycin on ribosome-catalysed peptidyl transfer. Nature *222*, 356–358.

Nierhaus, K.H., Schulze, H., and Cooperman, B.S. (1980). Molecular mechanisms of the ribosomal peptidyl transferase center. Biochem. Int. *1*, 185–192.

Nissen, P., Hansen, J., Ban, N., Moore, P.B., and Steitz, T.A. (2000). The structural basis of ribosome activity in peptide bond synthesis. Science *289*, 920–930.

Noller, H.F., Hoffarth, V., and Zimniak, L. (1992). Unusual resistance of peptidyltransferase to protein extraction procedures. Science *256*, 1416–1419.

Noller, H.F., Yusupov, M.M., Yusupova, G.Z., Baucom, A., and Cate, J.H.D. (2002). Translocation of tRNA during protein synthesis. FEBS Lett. *514*, 11–16.

Odom, O.W., Picking, W.D., and Hardesty, B. (1990). Movement of tRNA but not the nascent peptide during peptide bond formation on ribosomes. Biochemistry *29*, 10734–10744.

Ofengand, J., and Bakin, A. (1997). Mapping to nucleotide resolution of pseudouridine residues in large subunit ribosomal RNAs from representative eukaryotes, prokaryotes, archaebacteria, mitochondria, and chloroplasts. J. Mol Biol. *266*, 246–268.

Otwinowski, Z., and Minor, W. (1997). Processing of X-ray diffraction data collected in oscillation mode. Macromolecular Crystallogr. Pt A *276*, 307–326.

Pape, T., Wintermeyer, W., and Rodnina, M. (1999). Induced fit in initial selection and proofreading of aminoacyl-tRNA on the ribosome. EMBO J. *18*, 3800–3807.

Pestka, S. (1977). Inhibitors of protein synthesis. In Molecular Mechanisms of Protein Biosynthesis, H. Weissbach and S. Pestka, eds. (New York: Academic Press), pp. 467–553.

Polacek, N., Gaynor, M., Yassin, A., and Mankin, A.S. (2001). Ribosomal peptidyltransferase can withstand mutations at the putative catalytic nucleotide. Nature *411*, 498–501.

Porse, B.T., and Garrett, R.A. (1995). Mapping important nucleotides in the peptidyl transferase centre of 23 S rRNA using a random mutagenesis approach. J. Mol. Biol. *249*, 1–10.

Porse, B.T., Kirillov, S.V., Awayez, M.J., Ottenheijm, H.C., and Garrett, R.A. (1999). Direct crosslinking of the antitumor antibiotic sparsomycin, and its derivatives, to A2602 in the peptidyltransferase center of 23S-like rRNA within ribosome-tRNA complexes. Proc. Natl. Acad. Sci. USA *96*, 9003–9008.

Rheinberger, H.J., Sternbach, H., and Nierhaus, K.H. (1981). Three tRNA binding sites on *Escherichia coli* ribosomes. Proc. Natl. Acad. Sci. USA *78*, 5310–5314.

Rodriguez-Fonseca, C., Amils, R., and Garrett, R.A. (1995). Fine structure of the peptidyl transferase centre on 23S-like rRNAs deduced from chemical probing of antibiotic-ribosome complexes. J. Mol. Biol. *247*, 224–235.

Rodriguez-Fonseca, C., Phan, H., Long, K.S., Porse, B.T., Kirillov, S.V., Amils, R., and Garrett, R.A. (2000). Puromycin-rRNA interaction sites at the peptidyl transferase center. RNA *6*, 744–754.

Samaha, R.R., Green, R., and Noller, H.F. (1995). A base pair between tRNA and 23S rRNA in the peptidyltransferase centre of the ribosome. Nature *377*, 309–314.

Schluenzen, F., Zarivach, R., Harms, J., Bashan, A., Tocilj, A., Albrecht, R., Yonath, A., and Franceschi, F. (2001). Structural basis for the interaction of antibiotics with the peptidyl transferase centre in eubacteria. Nature *413*, 814–821.

Schmeing, T.M., Seila, A.C., Hansen, J.L., Freeborn, B., Soukup, J.K., Scaringe, S.A., Strobel, S.A., Moore, P.B., and Steitz, T.A. (2002). A pre-translocational intermediate in protein synthesis observed in crystals of enzymatically active 50S subunits. Nat. Struct. Biol. *9*, 225–230.

Shevack, A., Gewitz, H.S., Hennemann, B., Yonath, A., and Wittmann, H.G. (1985). Characterization and crystallization of ribosomal particles from *Halobacterium marismortui*. FEBS Lett. *184*, 68–71.

Smith, J.D., Traut, R.R., Blackburn, G.M., and Monro, R.E. (1965). Action of puromycin in polyadenylic acid-directed polylysine synthesis. J. Mol. Biol. *13*, 617–628.

Stark, H., Orlova, E.V., Rinke-Appel, J., Junke, N., Mueller, F., Rodnina, M., Wintermeyer, W., Brimacombe, R., and van Heel, M. (1997). Arrangement of tRNAs in pre- and posttranslocational ribosomes revealed by electron cryomicroscopy. Cell *88*, 19–28.

Tan, G.T., DeBlasio, A., and Mankin, A.S. (1996). Mutations in the peptidyltransferase center of 23S rRNA reveal the site of action of sparsomycin, a universal inhibitor of translation. J. Mol. Biol. *261*, 222–230.

Theocharis, D.A., and Coutsogeorgopoulos, C. (1992). Mechanism of action of sparsomycin in protein synthesis. Biochemistry *31*, 5861–5868.

Thompson, J., Kim, D.F., O'Connor, M., Lieberman, K.R., Bayfield, M.A., Gregory, S.T., Green, R., Noller, H.F., and Dahlberg, A.E. (2001). Analysis of mutations at residues A2451 and G2447 of 23S rRNA in the peptidyltransferase active site of the 50S ribosomal subunit. Proc. Natl. Acad. Sci. USA *98*, 9002–9007.

Traut, R.R., and Monro, R.E. (1964). The puromycin reaction and its relationship to protein synthesis. J. Mol. Biol. *10*, 63–72.

Vazquez, D. (1979). Inhibitors of protein biosynthesis. Mol. Biol. Biochem. Biophys. *30*, 1–312.

Vester, B., and Garrett, R.A. (1988). The importance of highly conserved nucleotides in the binding region of chloramphenicol at the peptidyltransfer center of *E. coli* 23S ribosomal RNA. EMBO J. *7*, 3577–3588.

Wilson, K.S., and Noller, H.F. (1998). Mapping the position of translational elongation factor EF-G in the ribosome by directed hydroxyl radical probing. Cell *92*, 131–139.

Yonath, A. (2002). The search and its outcome. Annu. Rev. Biophys. Biomol. Struct. *31*, 257–273.

Yusupov, M.M., Yusupova, G.Z., Baucom, A., Lieberman, K., Earnest, T.N., Cate, J.H., and Noller, H.F. (2001). Crystal structure of the ribosome at 5.5 Å resolution. Science *292*, 883–896.

Accession Numbers

The coordinates of the complexes were submitted to the PDB (accession codes 1NJM, 1NJN, 1NJP, and 1NJO).